OPEN ACCESS
IOP Publishing
Plasma Physics and Controlled Fusion
Plasma Phys. Control. Fusion **58** (2016) 084006 (5pp)
doi:10.1088/0741-3335/58/8/084006

Laboratory evidence for stationary inertial Alfvén waves

M E Koepke[1,4], S M Finnegan[1], S Vincena[2], D J Knudsen[3], S H Nogami[1] and D Vassiliadis[1]

[1] Department of Physics, West Virginia University, Morgantown, WV, USA
[2] Department of Physics and Astronomy, University of California, Los Angeles, CA, USA
[3] Department of Physics and Astronomy, University of Calgary, Alberta, Canada

E-mail: mark.koepke@mail.wvu.edu

Received 25 January 2016, revised 12 May 2016
Accepted for publication 26 May 2016
Published 15 July 2016

Abstract

Azimuthal convective flow and density-depleted magnetic field-aligned current co-located in the helium plasma produced in the large plasma device (LAPD-U) at UCLA (Gekelman *et al* 2016 *Rev. Sci. Instrum.* **87** 025105) support an Alfvénic perturbation that is static in the laboratory frame. Electrostatic probes measure the flow and static density perturbations in the 72 cm-diameter, 12 m-long, afterglow plasma, wherein a radially segmented electrode creates the convective flow and an off-cylindrical-axis planar-mesh electrode draws current in a channel parallel to the background magnetic field. This stationary 'wave' is measured as a fixed (in the laboratory frame) ion density structure.

Keywords: Alfven wave, auroral phenomena, space-related laboratory experiment

(Some figures may appear in colour only in the online journal)

Introduction and background

An Alfvén wave [1] is a perturbation, oscillatory in time, space, or both, of magnetic field strength B and plasma density n in magnetized plasma. While ubiquitous in nature, an Alfvén wave is difficult to study in the laboratory due to its relatively large spatial scale. An Alfvén wave can be studied in detail in a long plasma column at a few facilities around the world. We report results obtained in the large plasma device (LAPD-U) [2] during the multi-year Space Plasma Campaign [3] at UCLA's Basic Plasma Science Facility. The objective of the work reported here is to find a new mechanism for structure and flows in plasma that could be responsible for accelerated, energetic particles from enhanced Alfvénic coupling and transport of mass, momentum, and energy.

The aurora yields important clues about plasma and large-scale dynamic processes in the solar-terrestrial environment [4, 5]. Auroral arcs are understood to be a manifestation of geospace processes powered by interactions with the solar wind. The spatial characteristics of discrete auroral arcs (e.g. spatial extent, alignment, structure, etc) have been studied in detail for the past half-century (see [5]). In a separate study [6], we are examining the temporal characteristics of discrete auroral arcs. These studies help constrain models of auroral-arc generation. Knudsen [7] predicts the existence of a stationary inertial Alfvén (StIA) wave and connects the phenomenon to the observation of long-lifetime discrete auroral arcs. The free energy of a StIA wave is magnetic-field-aligned electron drift energy that overcomes collisional dissipation and collisionless phase mixing. Evidence of static, or quasi-static, parallel electric field generation has implications for the temporal characteristics of discrete auroral arcs. Here, we report the first laboratory evidence for StIA waves [8].

Auroral electron acceleration, from Alfvén-wave-induced formation of a parallel electric field and the consequent current-carrying population of energetic particles (particles with energies well above the typical 'thermal' energy of the system), is a key dynamic in the magnetosphere–ionosphere coupling in geospace, having applications to other magnetized planets such as Jupiter, or to any object with strongly

[4] Author to whom any correspondence should be addressed.

Table 1. Characteristics plasma parameters, frequencies, scale lengths, and velocities for LAPD and ionosphere [8]. The dimensionless quantity ω_{pe}/ω_{ce} ranges from 0.6 to 1.0 in the ionosphere and is approximately 4.5 in LAPD main discharge, 3.2 in LAPD afterglow, and 1.0 in ionosphere.

	LAPD plasma main discharge	LAPD plasma afterglow	Ionosphere (0.24 R_E altitude)
Ion species	Helium	Helium	Oxygen
n (cm^{-3}), density	2 ×,10^{12}	1 2,10^{11}	6 1,10^{3}
B_0 (G), field	1 (G10^{3}	1 0G10^{3}	0.26
T_e (eV), temp	6	0.6	1
T_i (eV), temp	1	0.5	1
ω_{pe} (rad s^{-1}), plasma freq	7.98 .910^{10}	5.64 .610^{10}	4.37 × 10^{6}
ω_{ce} (rad s^{-1}), cyc freq	1.76 × 10^{10}	1.76 × 10^{10}	4.57 × 10^{6}
ν_e (1/s), collision freq	4.56 × 10^{6}	5.27 × 10^{7}	0.25
ν_{in} (1/s), collision freq	86.2	60.9	0
λ_d (cm), Debye	1.3 × 10^{-3}	5.8 × 10^{-4}	9.59
λ_e (cm) $= c/\omega_{pe}$	0.38	0.53	6.8 × 10^{3}
$^{V}_{A}$ (cm s^{-1}), Alfven	7.73 × 10^{7}	1.1 × 10^{8}	1.8 × 10^{8}
βm, beta × ion/el mass ratio	4.11	0.32	0.2
τ, ion/electron temp ratio	0.17	1.2	1

convergent magnetic fields such as pulsar magnetospheres or astrophysical jets from active galactic nuclei.

Experimental device

The LAPD [3] is a linear-geometry, high-pulse-repetition plasma device that produces low-density, low-plasma-beta, helium or argon plasma. Plasma production occurs via ionization of a neutral gas by a 72 cm-diameter electron beam generated by a cathode–anode discharge at one end of the 18 m plasma column. The 1 m-diameter, 22 m-long vacuum vessel is surrounded by 90 solenoidal electromagnetic coils that produce the radially confining, axial magnetic field, the strength of which is adjustable up to 0.36 T. The LAPD plasma source [9] incorporates a 72 cm-diameter barium-oxide-coated cathode and grid-anode combination that can produce cylindrical plasmas up to 18 m long, 0.9 m wide, having densities up to 7×10^{12} cm^{-3} with a spatial uniformity of ±10%. We employ 13 m of this plasma column. The plasma is pulsed with a frequency of 1.000 Hz, with the duration of plasma production being variable from 10 ms to 20 ms. The transistor-switched plasma source produces extremely reproducible main-plasma and afterglow-plasma every discharge. Typical dimensional and dimensionless parameters for helium plasma in the LAPD are given in table 1. All of the experimental results reported here were performed in helium plasma.

Diagnostics include the current–voltage characteristic of an electrostatic (Langmuir) probe, the analysis of which yields information about the density, electron temperature, space potential of the plasma, and the vector components of flow velocity of ions in magnetized plasma. A Mach probe is an electrostatic probe designed to measure the vector components of flow velocity of ions in magnetized plasma. The probe is inserted radially into the plasma along the probe's rotation axis. The probe has a pair of one-sided planar collecting surfaces that face in opposite directions along the magnetic-field-aligned direction. In the case of bulk-plasma flow, current collected by the upstream-facing collecting surface is larger than the current collected by the downstream-facing collecting surface. The relationship between the upstream and downstream values of collection currents is [10]

$$\frac{1}{b}\ln\left[\frac{I_{i,\mathrm{sat}}(\theta)}{I_{i,\mathrm{sat}}(\theta+\pi)}\right]=\frac{V_{\parallel}-V_{\perp}\cot\theta}{C_S}.$$

Here, C_S is the ion sound speed, $\theta = \pi/2$ means the probe surface normal vector is aligned with the background magnetic field, and $b = 0.5$ is a common approximation of the experimentally determined empirical constant. The experimentally determined value of parallel flow, i.e. when $\theta = 0$, can be measured independently of the perpendicular flow. In order to calculate the perpendicular flow, the parallel flow must be known for any value of θ. Thus, the employed probe design utilizes additional pairs of collecting surfaces oriented around the cylindrical axis of the probe stem.

Off-axis, collimated magnetic-field-aligned (parallel) current is created by preferentially drawing electrons, with respect to the ions, to a mesh electrode (ME) biased positive with respect to the LAPD source anode or by thermionic electron emission from a hot circular cathode biased negative with respect to the LAPD source anode. In the case presented here, we use the former method, which corresponds to direction of parallel electron drift velocity being antiparallel to the direction of magnetic field. The divergence-free condition results in the in-channel current density being associated with reduced plasma density compared to the current-free, out-of-channel, ambient plasma.

Azimuthally-symmetric plasma rotation is controlled with an axially centered, multi-disk electrode (MDE) consisting of 9 aluminum disks (diameters range from 10.4 cm to 29.0 cm) having cylindrical axes and surface-normal vectors aligned with the magnetic field, stacked concentrically, separated electrically by ceramic spacers, held together with a single metal bolt, and differentially biased in two groups chosen to place the plasma-convection annulus at the preferred radius.

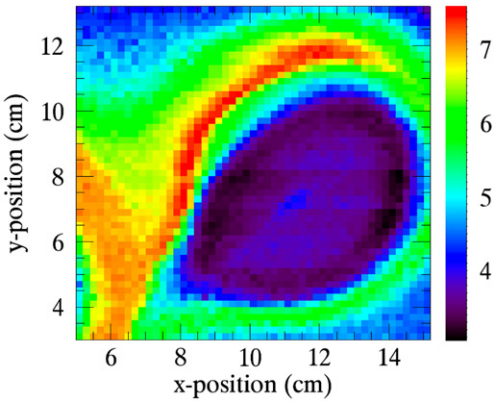

Figure 1. 2D plot of time-averaged ion saturation current, measured on the Mach probe collecting surface that face toward the plasma source, at $t = 1.03$ ms (after the discharge current has been terminated and both the MDE and ME are 'on'). Each square super-pixel represents the average ion saturation current measured over ten plasma discharges. The direction of the plasma rotation is clockwise. The MDE and ME biases are $V_{\mathrm{MDE}} = 420$ V and $V_{\mathrm{ME}} = 40$ V, respectively, with $B_0 = 1$ kG.

The plasma-column-end boundary potential profile is responsible for an annulus of $E \times B$ flow that extends axially many meters along the plasma column. The voltage applied to the MDE is supplied by a high-voltage (variable 0–420 V) pulsing circuit that allows the MDE bias to be switched on and off, on demand, during each plasma discharge.

To assess the 2D pattern of perturbations multiple times during a single discharge, the voltage applied to the MDE, placed 13 m from the source anode, is pulsed three times at $V_{\mathrm{MDE}} = 400$ V for 0.8 ms, each pulse being separated by 0.3 ms, with the first pulse initiated after the discharge current terminates. We select the best-timed pulse, with respect to the signal-to-noise ratio, indirectly selecting for the inertial regime and minimum collisional dissipation, for display and interpretation. Like the MDE, the voltage applied to the ME is also pulsed three times at $V_{\mathrm{ME}} = 40$ V for 0.6 ms duration, each pulse being separated by 0.5 ms, with the first pulse beginning 0.2 ms after the MDE pulse begins. Bias voltages to both the MDE and ME pulses are terminated simultaneously. Data is sampled at high frequency during this pulse train. The effects of Coulomb collisions become significant in the LAPD afterglow plasma (electron–ion collision frequency $\nu_{\mathrm{ei}} \propto T_{\mathrm{e}}^{-3/2}$). This is not a limitation, because collisionality and nonzero electron temperature have been incorporated into the model [11]. The inertial regime for Alfven waves exists when plasma beta is smaller than the electron–ion mass ratio. Operating LAPD at low magnetic field, the inertial regime is attainable in the afterglow-plasma as the electrons cool rapidly compared to the plasma-density decay.

StIA wave experiment

According to the theoretical model [7, 11], StIA wave structures should only exist in the presence of both the parallel current and plasma rotation. When the MDE is unbiased, the space potential is uniform across the diameter of the plasma, whereas when a voltage bias is applied to the MDE, the shape

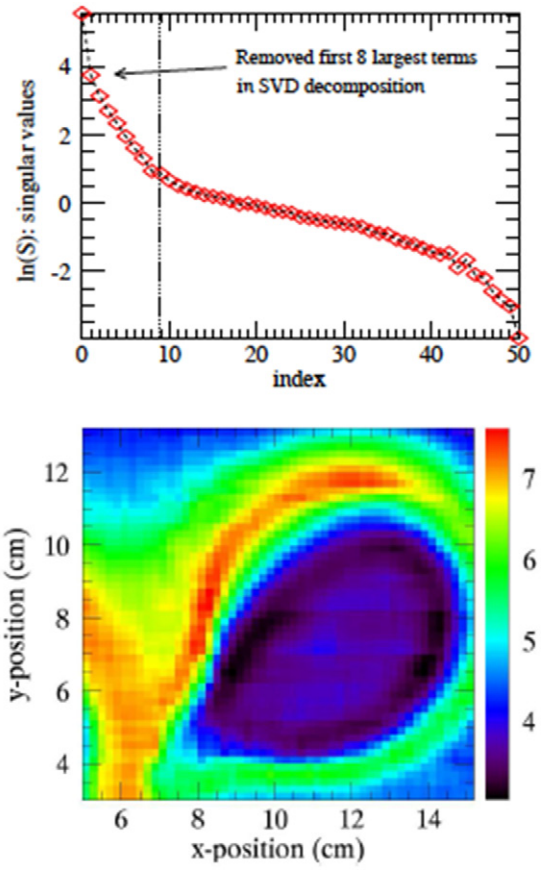

Figure 2. (*Top panel*) The singular value spectrum for the SVD of figure 1. (*Bottom panel*) The superposition of the first eight principle images, $A^{(8)} = \Sigma_{j=0\text{–}7}\, \sigma_j\, u_j\, v^T$. The dominant structures in the plasma density are recovered.

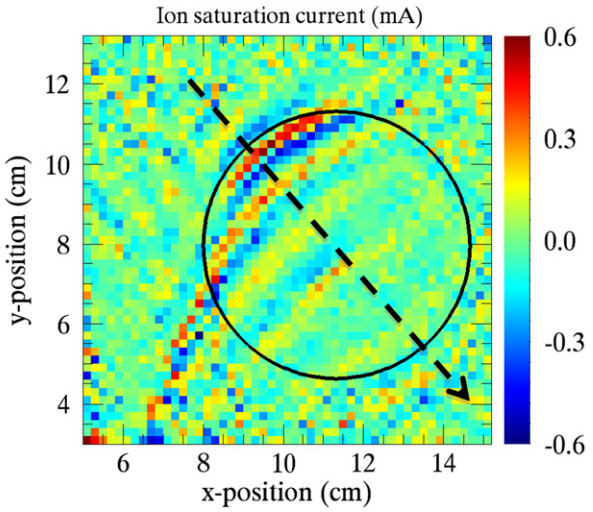

Figure 3. The large scale density structures are removed from figure 1, $A - A^{(8)}$, and what remains are fluctuations in the plasma density having wavefronts aligned with the direction of the rotational flow (clockwise), and collocated in the region of the ME (border outlined with a circle). Graphically, the wavelength of the observed density perturbations is determined to be approximately $\lambda_0 \approx 1.68\ \lambda_{\mathrm{e}}$.

of the space potential is peaked at the radial interface between the innermost and outermost groups of ganged plates [3]. The MDE is capable of producing controllable plasma drift across

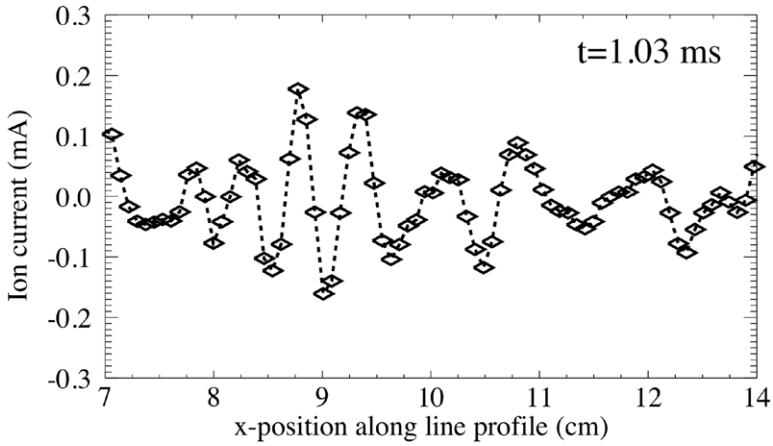

Figure 4. Linear interpolation of the measured values of ion saturation current lying along the dashed line in figure 3, plotted as a function of their *x*-coordinate.

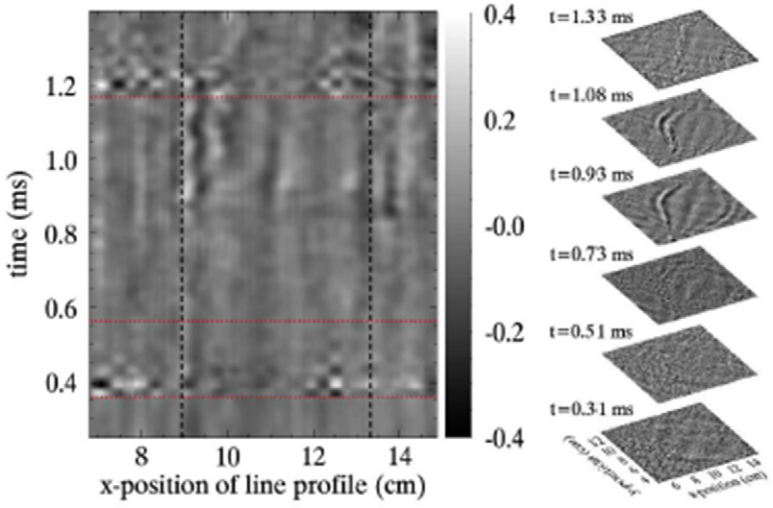

Figure 5. Evidence of a non-fluctuating, non-traveling pattern based on the spatial profile and time evolution of plasma density. (Right) Ion current measured along the dashed line seen in figure 3 is plotted as a function of time. The vertical dashed lines indicate the boundaries of the ME, and the horizontal lines indicate the initialization of the MDE pulse, ME pulse and pulse termination, respectively. During the period of time when both the MDE and ME are 'on' (0.56 ms $< t <$ 1.16 ms), a stationary pattern (sequence of vertical lines of constant amplitude which are periodic in *x*-position) forms on the downstream (relative to the direction of the cross-field flow) side of the ME boundaries.

the magnetic field, extending most of the experimentally relevant plasma column length. The plasma rotates during all three of the MDE/ME pulses.

The StIA wave pattern is seen in the 2D planes of ion-saturation current but only after the raw data (figure 1) is processed (figures 2 and 3) to remove the large-scale artifacts of the current channel and the probe translation to obtain the analyzed data (figures 3–5). Raw data is processed by IDL software. For small values of parallel electron flow speed, StIA wave perturbations in plasma density can be several orders of magnitude smaller than the background density, i.e. $\delta n/n \sim 1\%$. In order to resolve such small perturbations to the background plasma density, the 2D data array of ion-saturation current is decomposed using singular value decomposition (SVD) [8, 12], also known as principal-component analysis. Decomposing a principal image using SVD is similar to Fourier transforming a time series. The data 'image'-array can be represented as the linear superposition of weighted principal images (also called principal components). SVD is often utilized as a low pass filter to eliminate noise i.e. to make images sharper. We use SVD to remove dominant large-scale structures present in the image in order to reveal small amplitude structures that are otherwise obscured.

Laboratory observations of these StIAW patterns are consistent with the following predictions from the StIAW theory: (1) Perturbed region is co-located with the off-axis-current-channel and is absent elsewhere. (2) Perturbed pattern only exists in the simultaneous presence of both cross-field plasma flow and parallel current. (3) Perturbed 2D pattern is stationary (direct current) in the lab frame. (4) Perturbed amplitude versus distance along cross-field plasma flow maximizes immediately beyond the ambient-plasma/current-channel interface, in step-function fashion, and is spatially damped in the direction of the cross-field plasma flow. In the lab results,

these aspects are apparent in two dimensions at one axial position for one perturbed parameter and several values of each of the bulk parameters.

Plasma flow across a B-aligned current channel is predicted to generate periodic enhancements or depletions in the background plasma density, in the direction of the cross-field plasma flow. To see the StIA wave structure, the SVD spectrum is plotted (figure 2 (top)), the principal components corresponding to the 8 largest singular values are subtracted from the raw data image, the 2D image is reconstructed (figure 3), a wavefront-normal axis is chosen, and the wave signal along this wavefront-normal axis (figure 4) is plotted as a function of time in figure 5 (left). The rotation is turned on at 0.4 ms, the current is turned on at 0.6 ms, and both are turned off at 1.2 ms. Between 0.6 and 1.2 ms, the StIA wave pattern, obvious as vertical stripes, emerges in the 1D gray-scale line-out displayed in the space-time plot. 2D structure evolves in time, as seen in figure 5 (right). The perturbations form wavefronts with the wavefront-normal aligned with the direction of the rotational flow (clockwise). The wavelength of the observed density perturbation is $\lambda \approx 1.1$ cm. For $\lambda_e \approx 0.7$ cm, $\lambda/\lambda_e \approx 1.7$.

Discussion

Approximating the plasma density within the current channel at $t = 1.03$ ms in figures 3 and 5(left) to be 0.6×10^{12} cm^{-3}, the electron inertial length is approximately $\lambda_e \approx 0.7$ cm. The perturbation in the plasma density is predicted to have a perpendicular wavelength of approximately $50\lambda_e$, whereas the observed wavelength ($\lambda \approx 1.1$ cm) is on the order of λ_e. The structure exists only when both the convection and parallel current are present. The observed density structure could be interpreted as non-noise, fiducial, spatial inhomogeneity on top of the otherwise uniform ($n = 0$) StIA mode structure of the entire current channel, where n is the number of StIA perpendicular wavelengths across the current channel, in which case, the unambiguously stationary nature of the structure in time, approximately periodic nature of the structure in space, and the apparent damping of the structure by the time the structure extends to the destination-edge of the current channel (presumably by Coulomb collisions) is evidence for the StIA wave, even without additional quantitative mode-structure validation. Targeted validation experiment-theory comparisons are underway.

Conclusion

Time-stationary, self-excited, magnetized-plasma structure that arises in the perturbed plasma quantities is measured in the laboratory when a channel of magnetic-field-aligned (parallel) electron current and associated density depletion are co-located with cross-field plasma convection ($E \times B$ flow). These ingredients are responsible for laboratory evidence for the existence of StIA wave, presented here, and are being employed with the intention to validate stationary inertial Alfven wave (StIAW) theory [7, 10] in the laboratory.

Acknowledgments

This Space Plasma Campaign is supported by (NSF-PHYS-0613238 and NSF-PHYS-1301896). Experimental assistance from W Gekelman, J Maggs, B Van Compernolle, and S Tripathi (all at UCLA) is gratefully acknowledged. This Space Plasma Campaign is being carried out by M Koepke, D Knudsen, P Damiano, J Johnson, R Rankin, R Marchand, C Chaston and S Vincena at the Basic Plasma Science Facility (BAPSF), University of California, Los Angeles, and thus receives part of the BAPSF facilities support from NSF and DoE. DK's participation is supported by a grant from the Natural Sciences and Engineering Council of Canada.

References

[1] Alfvén H 1942 *Nature* **150** 405
[2] Gekelman W *et al* 2016 *Rev. Sci. Instrum.* **87** 025105
[3] Koepke M E, Finnegan S M, Vincena S, Knudsen D J and Chaston C 2008 *Plasma Phys. Control. Fusion* **50** 074004
[4] Karlsson T and Marklund G T 1996 *Geophys. Res. Lett.* **23** 1005
[5] Sandahl I, Sergienko T and Brändström U 2008 Fine structure of optical aurora *J. Atmos. Sol.-Terr. Phys.* **70** 2275–92
[6] Nogami S H 2015 Basic plasma science facility (BaPSF) space plasma campaign: space observation (invited talk) *Int. Workshop on the Interrelationship between Plasma Experiments in the Laboratory and in Space (IPELS) (Pitlochry, UK, 24–28 August 2015)*
[7] Knudsen D J 1996 *J. Geophys. Res.* **101** 10761
[8] Finnegan S M 2008 The stationary Alfvén wave in laboratory and space regimes *PhD Dissertation* Department of Physics, West Virginia University http://hdl.handle.net/10450/5933
[9] Leneman D, Gekelman W and Maggs J 2006 *Rev. Sci. Instrum.* **77** 015108
[10] Van Goubergen H, Weynants R R, Jachmich S, Van Schoor M, Van Oost G and Desoppere E 1999 *Plasma Phys. Control. Fusion* **41** L17
[11] Finnegan S M, Koepke M E and Knudsen D J 2008 *Phys. Plasmas* **15** 052108
Finnegan S M, Koepke M E and Knudsen D J 2008 *Plasma Phys. Control. Fusion* **50** 074005
Finnegan S M, Koepke M E and Knudsen D J 2008 *Nonlinear Process. Geophys.* **15** 957
[12] Press W H, Flannery B P, Teukolsky S A and Vetterling W T 1992 *Numerical Recipes* 2nd edn (Cambridge: Cambridge University Press)